Boron reactivation kinetics in hydrogenated silicon after annealing in the dark or under illumination

T. Zundel and J. Weber
Max-Planck-Institut für Festkörperforschung, Heisenbergstrasse 1, D-7000 Stuttgart 80, Federal Republic of Germany
(Received 13 August 1990)

The reactivation kinetics of passivated boron in hydrogenated silicon are studied systematically with respect to temperature, acceptor concentration, and illumination. The change of the net inactive boron concentration R versus annealing time t satisfies the equation $dR/dt = -rR^2/(N_A - R)^2$, where N_A is the total boron concentration. The annealing parameter r does not depend on N_A, but shows a linear dependence on the optically generated electron concentration, provided the light intensity exceeds a threshold value. The annealing process is rate limited by the formation of a stable electrically inactive complex $\tilde{H}_2$, which involves two H atoms. The formation of $\tilde{H}_2$ strongly depends on the charge state of H, which is controlled by a H donor level located in the upper half of the band gap.

I. INTRODUCTION

Atomic hydrogen readily diffuses into crystalline silicon, and removes from the band gap most of the energy levels associated with a wide variety of chemical impurities or crystallographic defects.[1,2] The passivation of the group-III shallow acceptors A (A=B, Al, Ga, In, and Tl) has been intensively studied by infrared[3–9] and Raman[10–12] spectroscopy, photoluminescence,[13] channeling techniques,[14,15] perturbed angular correlation measurements,[16] and theoretical methods.[17–22] An electrically inactive acceptor-hydrogen complex (AH) is formed, with the H atom located near a bond-center (BC) position between the acceptor and one of its nearest silicon neighbors.[3–22]

The thermal reactivation of the passivated boron follows first-order kinetics in the space-charge region of a *reverse-biased* Schottky diode.[23] The analysis of the kinetics leads to a dissociation energy of the BH complex of $E_D = 1.28$ eV. In contrast, the B reactivation at *zero bias* shows a more complex behavior. A rapid initial step is followed by a slower thermally activated second-order process.[24–26] Sah *et al.*[25] proposed a model where the initial step is controlled by the trapping and detrapping of H at the acceptor, and the second-order process is explained by the formation and dissociation of H_2 molecules.

There is, however, only indirect experimental evidence for the existence of molecular hydrogen in silicon, due to the presumed electrical, optical, and paramagnetic inactivity of this species. Johnson *et al.*[27] after annealing of n^+p junctions under reverse bias found an accumulation of hydrogen in the p-type material near the edge of the depletion layer. The H-related species in that region are neutral, immobile, and stable up to 200 °C, and were proposed as molecular hydrogen H_2 which forms according to the reaction $H^+ + H^0 \rightarrow H_2 + h^+$. The formation of immobile H_2 molecules is also assumed to explain the anomalous decrease of the effective H diffusivity at temperatures below 500 °C.[28–31] The theoretical studies[18,32–35] predict that H_2 is located at a tetrahedral (T) interstitial site. The molecule is more stable than two noninteracting interstitial H atoms in their equilibrium positions,[18,33–36] except for Ref. 32 where the molecule is slightly less stable. Several other electrically inactive complexes involving two H atoms are theoretically studied in Refs. 18, 37, and 38.

The isolated interstitial hydrogen is difficult to detect because this species preferentially binds to defects or forms molecules. Channeling measurements[39] in deuterium-implanted high-resistivity Si reveal that most of the deuterium atoms are located close to bond-center sites after annealing. Gorelkinskii and Nevinnyi[40] detect an electron spin resonance (ESR) spectrum (labeled Si-*AA*9) in H-implanted silicon, which is consistent with BC-interstitial hydrogen. The hyperfine interaction of the Si-*AA*9 center is similar to that of anomalous muonium, a neutral pseudo-isotope of hydrogen located at the bond center.[41] Recent theoretical studies[32,33,42–44] also predict an equilibrium position at[32,33,42] or close[43,44] to the BC site for neutral interstitial H in defect-free silicon.

The positive charge state of interstitial H in p-type Si is demonstrated unambiguously by the drift of H in an electric field.[23,26,27,45–47] The dependence of the H diffusivity,[28,48,49] solubility,[50] and the H_2-molecule formation kinetics[27,50] on the conductivity-type and Fermi-level position provide indirect evidence for the neutral and negative charge states. The donor and acceptor levels associated with these charge states have never been detected in any optical or electrical measurement. Theoretical investigations[33] predict that positively charged hydrogen at the BC site is favored in p-type Si. Neutral hydrogen H^0 also occupies the BC site whereas H^- in n-type Si has the most stable position at the tetrahedral interstitial lattice position.[33] Van de Walle *et al.*[33] suggest that H forms a center with negative correlation energy U, but

the inaccuracies of the calculations do not definitively exclude a positive U center.

There is only minor evidence for the influence of light on the properties of hydrogen.[46,47] The passivation of the boron acceptor, which occurs when samples are boiled in water, is inhibited if the treatment is performed under strong illumination.[46] Tavendale *et al.*[47] mention that the thermal reactivation of the passivated boron is enhanced under illumination. These properties have not been investigated in detail and remain unexplained.

In this work we investigate in detail the reactivation of the H-passivated boron after annealing in the dark or under illumination. We show that the kinetics are rate limited by the recombination of two H atoms in a bimolecular $\tilde{H}_2$ species whose formation is strongly enhanced under illumination. Our investigations give new insight into the charge states of H and the H-related donor level. Section II provides the details of the experimental procedure. The experimental data are presented in Sec. III, analyzed in Sec. IV, and discussed in Sec. V.

II. EXPERIMENTAL DETAILS

Boron-doped (100) float-zone silicon samples of 120, 3.5, or 0.45 Ω cm resistivity are exposed for 2 h to a radio frequency (13 MHz) driven hydrogen plasma at a temperature in the range of 110 to 130 °C. The samples are then boiled in nitric acid for 1 min, and semitransparent titanium Schottky contacts (1 mm diameter, ≈40 nm thickness) are evaporated onto the surface that is exposed to the plasma. The ohmic contact consists of an indium-gallium alloy scratched onto the back surface. Capacitance versus voltage [$C(V)$] measurements at 1 MHz and room temperature provide the concentration profile $N_I(x)$ of the net electrically active boron acceptor, i.e., the net charge of both the negative acceptor and the positively charged hydrogen. The thin oxide layer (2 nm) produced by the nitric acid treatment has a negligible influence on the $C(V)$ measurements, but lowers the dark saturation current I_0 of the diode ($I_0 \sim 10^{-1}$ μA at 300 K).

Anneals carried out at a temperature T_a in the range 100–200 °C are performed under ambient atmosphere. After annealing for a time t_a, the temperature is rapidly decreased to room temperature by briefly immersing the sample holder in liquid nitrogen. For the anneals under illumination, a monochromatic light beam ($\lambda = 802$ nm) from a Ga-Al-As power laser diode is focused onto the Schottky contact. In order to minimize edge effects, we set the diameter of the light spot (≈3 mm) larger than the titanium dot. We monitor the incident light intensity ϕ by measuring the photocurrent I_{ph} of the diode at room temperature. Due to the series resistance,[51] the current $I(\phi, V_R)$ flowing across the reverse-biased diode increases with the reverse voltage V_R, and saturates at $I_s(\phi) = I_{ph} - I_0$. In the investigated range ($I_{ph} = 10^{-4}$–10 mA), I_{ph} is rigorously proportional to the incident light intensity ϕ measured with a power meter I_{ph} ($\phi = \gamma I_{ph}$, with $\gamma = 196$ mW cm^{-2} mA^{-1}). Photocurrents larger than 1 mA are achieved by substituting the laser diode for a dye laser set to the same wavelength. The anneals under light are performed with the diode in the *open-circuit* configuration. The light remains off during the heating and cooling steps.

The following test is performed in order to rule out an increase of the sample temperature due to the light intensity. The temperature is stabilized at 100 °C, the lowest value used in our experiments. When light of the highest intensity ($I_{ph} = 10$ mA) hits the diode at $t = 0$, the open-circuit voltage reaches a stable value within less than 1 s, and remains stable as t further increases. The open circuit V_{oc} is very sensitive to the sample temperature, and a temperature increase of only 1 K would produce a measurable decrease of V_{oc}.

III. RESULTS

We systematically analyze the boron reactivation kinetics as a function of the temperature ($T_a = 100$–200 °C) and the photocurrent I_{ph} in samples with various acceptor concentrations ($N_A = 1.1 \times 10^{14}$ cm^{-3}, 4.0×10^{15} cm^{-3}, 3.8×10^{16} cm^{-3}).

A. Determination of the annealing kinetics in the dark

A hydrogenated sample with resistivity 0.47 Ω cm is annealed in dark at a temperature $T_a = 160$ °C. The net electrically active boron profiles are shown in Fig. 1 for various annealing times t_a. As t_a increases, the dopant is progressively reactivated, and the profile of the control sample is restored for $t_a \sim 100$ h. The boron reactivation shows a negligible dependence on the depth x. In order to quantitatively analyze the reactivation process, we consider the inactive net acceptor concentration $R(t_a) = N_A - N_I$, where N_A represents the uniform boron concentration in the nonhydrogenated control sample. We first check if $R(t_a)$ satisfies equations

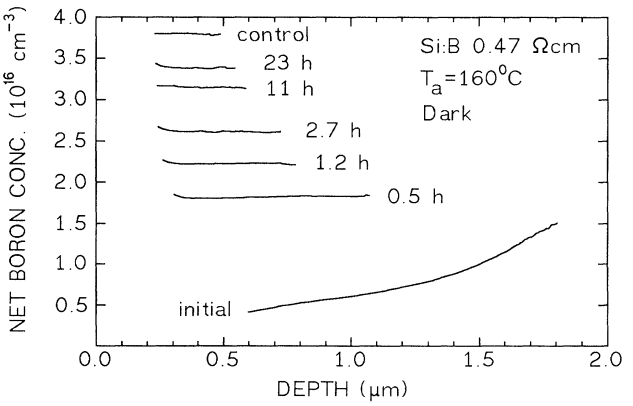

FIG. 1. Net active boron concentration profiles in a 0.47-Ω cm hydrogenated sample after annealing in the dark at $T_a = 160$ °C for various times. The profiles labeled control and initial are measured before and just after the H plasma exposure, respectively.

$\ln R(t_a) = -r'' t_a + \ln R_0$ and $R^{-1}(t_a) = r' t_a + R_0^{-1}$ which are obtained by integrating the following first- and second-order equations:

$$\frac{dR}{dt} = -r'' R \ , \tag{1}$$

$$\frac{dR}{dt} = -r' R^2 \ , \tag{2}$$

respectively. The parameters r'' and r' represent the first- and second-order annealing parameters, and R_0 equals $R(t_a = 0)$. We find that $\ln R(t_a)$ versus t_a strongly deviates from a linear relationship, e.g., the reactivation process does *not* follow first-order kinetics. The plot of $R^{-1}(t_a)$ versus t_a is shown in Fig. 2 (left-hand side scale, crosses). For $t_a > 3$ h, the data lie on a straight line whose slope corresponds to the second-order parameter $r' = 2 \times 10^{-21}$ cm^3/s. At short times, however, the boron reactivates at a faster rate than predicted by the second-order process.

The kinetic model we will develop in Sec. IV B predicts the following kinetic equation:

$$\frac{dR}{dt} = -r \frac{R^2}{(N_A - R)^2} \ , \tag{3}$$

where r is the annealing parameter. The integral form of Eq. (3) is

$$S(t_a) = r t_a + S(t_a = 0)$$

with

$$S = N_A^2 / R + 2 N_A \ln R - R \ .$$

As shown in Fig. 2 (right-hand side scale, squares), the experimental values of $S(t_a)$ vary linearly with t_a over the entire annealing process. The slope of the solid line gives the kinetic parameter $r = 1.5 \times 10^{12}$ cm^{-3}/s. Various values of the exponent of $(N_A - R)$ in Eq. (3), e.g., $\frac{1}{2}, 1, 3$, are investigated, but the quadratic dependence agrees best with the data.

We perform a similar experiment on a sample with a much lower acceptor concentration, which allows us to measure the dopant profile over a large depth range. The $C(V)$ profile recorded in a sample with $N_A = 1.1 \times 10^{14}$ cm^{-3} annealed in dark at $T_a = 160$ °C is shown in Fig. 3 for different annealing times t_a. The weak downward curvature of the profile at $x \approx 5$ μm also occurs in the control sample, and is an artifact of the measurement. The dopant is rapidly reactivated in the hydrogenated layer which extends up to ≈ 14 μm in the unannealed sample. The weak decrease of the boron concentration at $x > 12$ μm (Fig. 3) might be due to some in-diffusion of H from the region $x < 12$ μm, but the amount of H involved in this passivation is negligible compared to the amount of B which is reactivated in the region $x < 12$ μm. We conclude that the B reactivation is not diffusion limited. We determine the annealing parameters $r' = 7 \times 10^{-17}$ cm^3/s and $r = 7 \times 10^{11}$ cm^{-3}/s from the plots of R^{-1} and S versus t_a shown in Fig. 4. The values of r and r' do not depend on the depth w at which N_I is measured, for w in the range from 7 to 12 μm. The parameter r is close to the value determined in the 0.47-Ω cm sample (1.5×10^{12} cm^{-3}/s).

The boron reactivation is much faster in samples with a smaller doping concentration. The time to reactivate 90% of the boron acceptor in the specimens with $N_A = 1.1 \times 10^{14}$ cm^{-3} and $N_A = 3.8 \times 10^{16}$ cm^{-3} is ~20 min and ~23 h, respectively. (See Figs. 1 and 3.) However, the difference between the rates $r = 7 \times 10^{11}$ cm^{-3}/s and $r = 1.5 \times 10^{12}$ cm^{-3}/s determined in the samples with $N_A = 3.8 \times 10^{16}$ cm^{-3} and $N_A = 1.1 \times 10^{14}$ cm^{-3}/s is within the experimental accuracy of 80%. (See Sec. III D.) Therefore, the denominator $(N_A - R)^2$ in Eq. (3) fully accounts for the dependence of the annealing process on the acceptor concentration. In contrast, if we analyze the data according to the second-order model, we find that r' is inversely proportional to N_A^2, in agreement with the relation $r' = r / N_A^2$ derived from Eqs. (2) and (3)

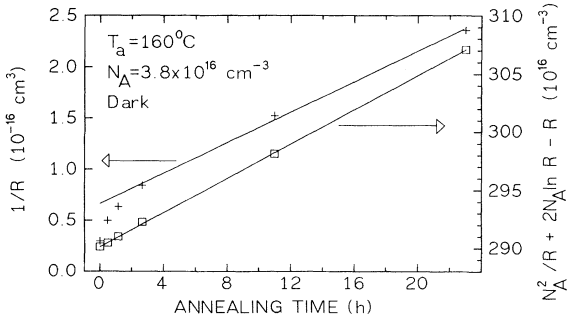

FIG. 2. Analysis of the annealing kinetics based on Eq. (2) (crosses, left-hand-side scale) and Eq. (3) (squares, right-hand-side scale). The parameter R is the net inactive boron concentration determined from Fig. 1 at a depth $w = 0.4$ μm. The solid lines represent the fit of the data to Eqs. (2) and (3) with $r' = 2 \times 10^{-21}$ cm^3/s and $r = 1.5 \times 10^{12}$ cm^{-3}/s.

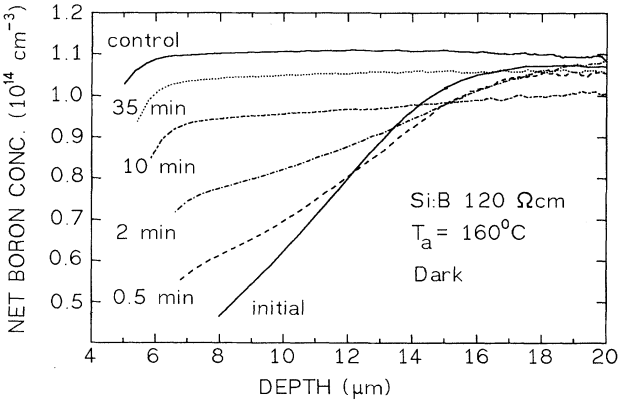

FIG. 3. Net active boron concentration profiles in a 120-Ω cm hydrogenated sample after annealing in the dark at $T_a = 160$ °C for different times. The profiles labeled control and initial are measured before and just after the H plasma exposure, respectively.

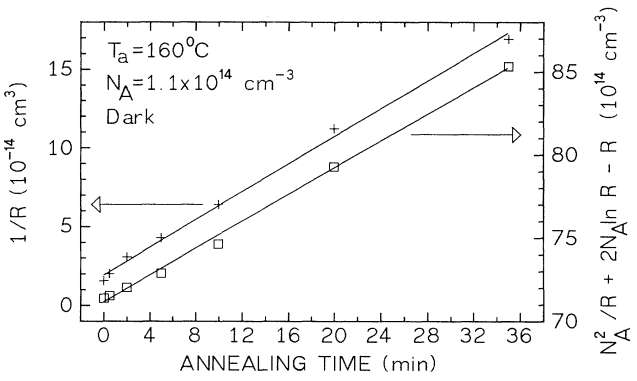

FIG. 4. Analysis of the annealing kinetics based on Eq. (2) (crosses, left-hand-side scale) and Eq. (3) (squares, right-hand-side scale). The parameter R is the net inactive boron concentration determined from Fig. 3 at a depth $w=8$ μm. The solid lines represent the fit of the data to Eqs. (2) and (3) with $r'=7\times10^{-17}$ cm^3/s and $r=7\times10^{11}$ cm^{-3}/s.

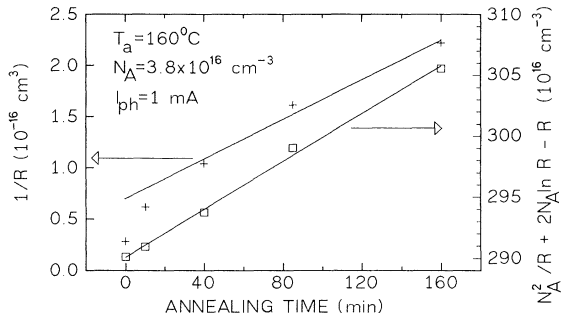

FIG. 6. Analysis of the annealing kinetics based on Eq. (2) (crosses, left-hand-side scale) and Eq. (3) (squares, right-hand-side scale). The parameter R is the net inactive boron concentration determined from Fig. 5 at a depth $w=0.4$ μm. The solid lines represent the fit of the data to Eqs. (2) and (3) with $r'=1.6\times10^{-20}$ cm^3/s and $r=1.6\times10^{13}$ cm^{-3}/s.

for $R \ll N_A$ (long annealing times). In summary, Eq. (3) fully describes the t_a and N_A dependence of the annealing process, and the annealing parameter r shows a negligible dependence on N_A.

B. Enhancement of the annealing kinetics under illumination

A 0.47-Ω cm sample is annealed at $T_a=160$ °C under light with an intensity corresponding to $I_{ph}=1$ mA. The acceptor profiles are shown in Fig. 5 for different annealing times t_a. The depth-independent reactivation of the acceptor is qualitatively similar to that observed in the dark (Fig. 1). The illumination, however, drastically enhances the annealing process. The time to reactivate 90% of the boron decreases from 23 h in the dark to 160 min under illumination. The analysis of the data based on Eqs. (2) and (3) is shown in Fig. 6. The kinetics deviate from second order for $t_a<40$ min (Fig. 6, crosses), but rigorously satisfy Eq. (3) throughout the entire time of annealing (Fig. 6, squares). The annealing parameter $r=1.6\times10^{13}$ cm^{-3}/s exceeds the value in the dark ($r=1.5\times10^{12}$ cm^{-3}/s) by one order of magnitude.

We perform similar experiments in the dark or under illumination for various values of T_a, N_A, and I_{ph}. At any investigated condition, the changes in the profiles are qualitatively similar to those shown in Figs. 1, 3, and 5, and the kinetics exactly satisfy Eq. (3). The dependence of r on I_{ph}, T_a, and N_A is presented in Sec. III C.

C. Dependence of r on I_{ph}, T_a, and N_A

Figures 7 and 8 (triangles) show double logarithmic plots of r versus I_{ph} for various acceptor concentrations,

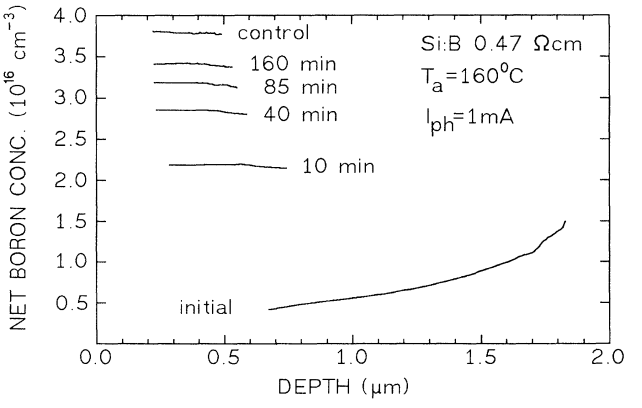

FIG. 5. Net active boron concentration profiles in a 0.47-Ω cm hydrogenated sample after annealing under illumination at $T_a=160$ °C for various times. The profiles labeled control and initial are measured before and just after the H plasma exposure, respectively.

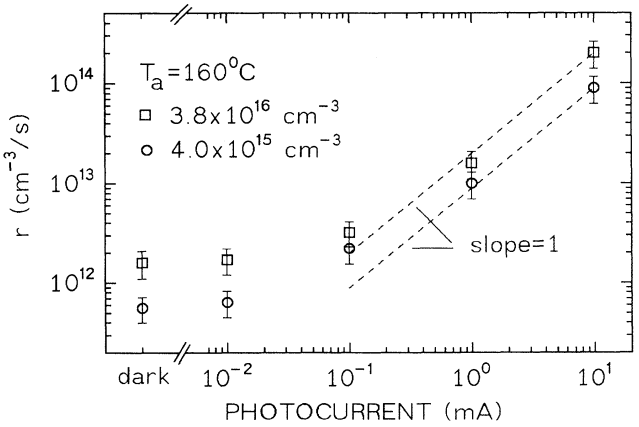

FIG. 7. Annealing parameter at $T_a=160$ °C as a function of the photocurrent for different total boron concentrations N_A.

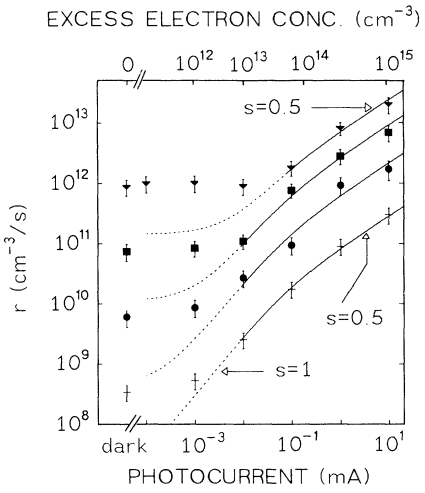

FIG. 8. Annealing parameter as a function of the photocurrent at various temperatures in a sample with $N_A=1.1\times10^{14}$ cm^{-3} (crosses, 100 °C; dots, 120 °C; squares, 140 °C; triangles, 160 °C). The slopes $s=1$ and 0.5 are shown by arrows. The upper scale shows the electron concentration calculated from Eqs. (4), (5), and (6) with $\tau_l=4$ μs and $\tau_h=0.4$ μs. The dashed or solid lines are calculated according to the equation $r=cn$, where c is an adjustable parameter plotted in Fig. 12. The lines are solid over the I_{ph} interval for which the fit is performed.

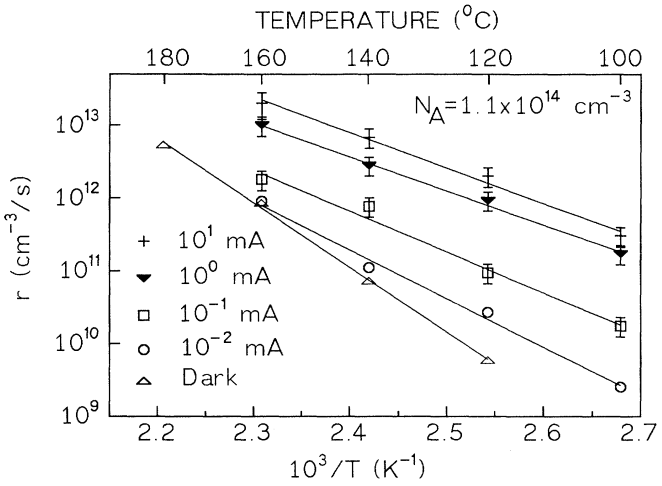

FIG. 9. Arrhenius plot of the annealing parameter in the dark and for various values of the photocurrent I_{ph} at a fixed boron concentration $N_A=1.1\times10^{14}$ cm^{-3}.

and at a fixed temperature $T_a=160$ °C. The kinetic parameter r strongly increases if the photocurrent exceeds a threshold value $I_{ph}^{th}\simeq10^{-2}$ mA. In the range from 1 to 10 mA, r varies linearly with I_{ph} in the more highly doped samples ($N_A=4.0\times10^{15}$ cm^{-3} and $N_A=3.8\times10^{16}$ cm^{-3}), and is proportional to $(I_{ph})^{1/2}$ in the lower doped sample ($N_A=1.1\times10^{14}$ cm^{-3}).

The dependence of r on I_{ph} at various other temperatures in the range 100–160 °C is shown in Fig. 8 for $N_A=1.1\times10^{14}$ cm^{-3}. The square-root dependence of r on I_{ph} occurs at all temperatures for $I_{ph}\geq1$ mA. A linear regime is observed for $T_a<160$ °C, and I_{ph} in the range from 10^{-2} to 10^{-1} mA.

The annealing parameter strongly increases with temperature. The Arrhenius plots of r for various values of I_{ph} in the range from 0 to 10 mA are shown in Fig. 9 for $N_A=1.1\times10^{14}$ cm^{-3}. The solid lines are obtained by fitting the experimental data to the relation $r=r_0\exp(-E_a/kT_a)$. The adjusted parameters E_a and r_0 are shown in Table I. As the light intensity increases, the activation energy E_a strongly decreases from the dark value $E_a^d=1.76\pm0.05$ eV, and saturates at $E_a^l=1.1\pm0.1$ eV for $I_{ph}\geq10^{-1}$ mA. At the same time the prefactor r_0 is lowered by about seven orders of magnitude.

The Arrhenius plots of r in the dark and under illumination ($I_{ph}=1$ mA) are shown in Figs. 10 and 11 for different values of N_A. The annealing parameter does not monotonically depend on N_A, and the scattering of $\sim80\%$ on the values of r corresponding to the various values of N_A is within the experimental error. (See Sec. III D.) These results confirm that r has only a negligible dependence on N_A. Table II displays the value of the adjusted parameters E_a and r_0. The activation energies averaged over the three values of N_A are $\bar{E}_a^d=1.75\pm0.06$ eV in the dark, and $\bar{E}_a^l=1.1\pm0.1$ eV for $I_{ph}=1$ mA.

D. Influence of the experimental conditions on the annealing kinetics

The measurements of r at a fixed value of N_A are performed on samples cut from the same wafer after the Schottky contact evaporation, but the wafers correspond-

TABLE I. Activation energies E_a and prefactor r_0 obtained by fitting the experimental values of r to equation $r=r_0\exp(-E_a/kT_a)$ for various values of the photocurrent I_{ph}. The acceptor concentration is $N_A=1.1\times10^{14}$ cm^{-3}.

I_{ph} (mA)	10^{1}	10^{0}	10^{-1}	10^{-2}	Dark
E_a (eV)	0.97±0.08	0.93±0.05	1.12±0.1	1.32±0.08	1.76±0.05
r_0 (cm^{-3}/s)	$(4^{+24}_{-3})\times10^{24}$	$(7^{+15}_{-5})\times10^{23}$	$(2.3^{+50}_{-2})\times10^{25}$	$(2.1^{+21}_{-2})\times10^{27}$	$(2^{+6}_{-1})\times10^{32}$

TABLE II. Activation energy E_A and prefactor r_0 of the kinetic parameter $r=r_0\exp(-E_a/kT)$ in samples with various acceptor concentrations N_A annealed in the dark or under illumination.

	Dark		$I_{ph}=1$ mA	
N_A (cm^{-3})	E_a (eV)	r_0 (cm^{-3}/s)	E_a (eV)	r_0 (cm^{-3}/s)
4.0×10^{15}	1.79±0.04	$(3^{+7}_{-2})\times10^{32}$	1.20±0.06	$(1.4^{+4}_{-1})\times10^{27}$
3.8×10^{16}	1.71±0.06	$(1.1^{+5}_{-1})\times10^{32}$	1.14±0.07	$(2.1^{+9}_{-2})\times10^{26}$
1.1×10^{14}	1.76±0.05	$(2^{+6}_{-1})\times10^{32}$	0.93±0.05	$(7^{+15}_{-5})\times10^{23}$

ing to different values of N_A are processed separately (hydrogenation, oxydation, contact evaporation). To estimate the error on the annealing parameter, we determine r at $T_a=120\,^\circ$C, $I_{ph}=1$ mA, $N_A=1.1\times10^{14}$ cm^{-3}, using two sets of four samples. The set I consists of samples cut from the same wafer after the contact evaporation, while the specimens of the set II are processed separately. The scattering of r in case I is ≈30% (error bars in Figs. 7, 8, and 9) and mainly results from the error on the net acceptor concentration N_I. The dispersion increases up to 80% under condition II, probably due to insufficient control of the processing conditions. We conclude that the values of r plotted in Figs. 10 and 11 do not show a significant dependence on N_A.

In the experiments described above, the anneals are performed in the open-circuit configuration, and the samples are *oxidized* in nitric acid prior to the evaporation of the Schottky contacts. We now investigate the influence of these two conditions on the annealing process.

A sample with $N_A=4.0\times10^{15}$ cm^{-3} is isothermally annealed at 80 °C under illumination ($I_{ph}=1$ mA), and with a reverse bias $V_R=60$ V applied to the diode. We observe the same changes in the acceptor profiles as reported in Ref. 23, for a similar experiment performed in the dark. (See Ref. 23, Fig. 1.) Due to the drift property of H, the reactivation of the acceptor in the space-charge region is limited by the dissociation of the boron-hydrogen complex, and follows first-order kinetics, which is characterized by the dissociation frequency[23] $\nu_{BH}=1.4\pm10^{-4}$ s^{-1}. We conclude that light has a negligible influence on the acceptor reactivation process for annealing under reverse bias.

An anneal with the diode in the *short-circuit* configuration is performed on a 120-Ω cm sample at $T_a=100\,^\circ$C, and $I_{ph}=1$ mA. The acceptor reactivation still follows the kinetics defined by Eq. (3), but the annealing parameter r is one order of magnitude smaller than the value measured in the open-circuit configuration.

We determine the dependence of r on I_{ph} at $T_a=120\,^\circ$C in 120-Ω cm samples, which are *not oxidized* prior to the Schottky contact evaporation. The dependence of r on I_{ph} is similar to that depicted in Fig. 8, but the values of r are four times lower than in the oxidized samples.

The following conclusions clearly emerge.

(1) The annealing kinetics of BH complexes in the dark and under illumination follow Eq. (3), and the annealing parameter r does not depend on the acceptor concentration N_A.

(2) The annealing parameter r strongly increases under illumination. In the higher doped samples ($N_A\geq4\times10^{15}$ cm^{-3}), r varies linearly with I_{ph} under strong illumina-

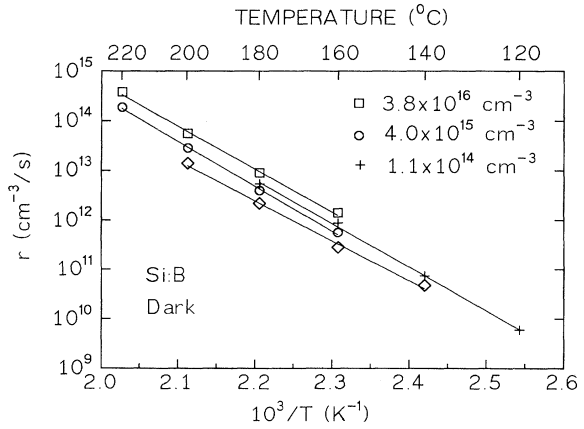

FIG. 10. Arrhenius plot of the annealing parameter in the dark for various values N_A. The rhombuses represent the product $r'N_A^2$, where r' is the second-order parameter determined in the H-implanted samples of Ref. 26 ($N_A=1.5\times10^{15}$ cm^{-3}).

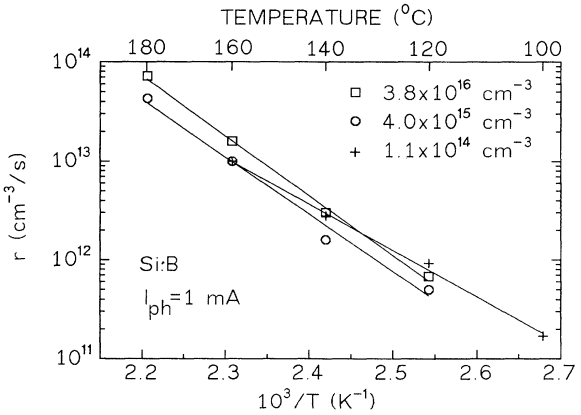

FIG. 11. Arrhenius plot of the annealing parameter under illumination ($I_{ph}=1$ mA) for different values N_A.

tion ($I_{ph} \geq 1$ mA). In the less doped samples ($N_A = 1.1 \times 10^{14}$ cm^{-3}), r linearly depends on I_{ph} for I_{ph} ranging from 10^{-2} to 10^{-1} mA, and is proportional to $(I_{ph})^{1/2}$ for $I_{ph} \geq 1$ mA.

(3) The parameter r is thermally activated. As I_{ph} increases, the activation energy E_a strongly decreases from the dark value $\bar{E}_a^d = 1.75 \pm 0.06$ eV, and saturates at $\bar{E}_a^l = 1.1 \pm 0.1$ eV for $I_{ph} \geq 10^{-1}$ mA.

(4) The second-order rate r strongly decreases if the anneals are performed in the short-circuit configuration, or if the samples are not oxidized in HNO_3 prior to the Schottky contact evaporation.

IV. ANALYSIS OF THE RESULTS

We now put forward a model that accounts for observations (1)–(4) of Sec. III. The light with energy $h\nu = 1.54$ eV generates electron-hole pairs. The negligible dependence of r on N_A, i.e., the hole concentration, suggests that the enhancement of r under illumination is controlled by the electron concentration n. Our first step is to derive a relation between n and the experimentally measured photocurrent I_{ph} (Sec. IV A). We will show that the linear or the square-root dependence of r on I_{ph} fully supports that r is proportional to n under illumination. In Sec. IV B we present an annealing mechanism which is consistent with Eq. (3), and we derive an expression of r in the dark and under illumination. The model is quantitatively compared to the experimental data in Sec. IV C.

A. Dependence of r on the electron concentration

In moderately doped silicon ($N_A < 10^{17}$ cm^{-3}), the electron-hole pairs predominantly recombine via the Shockley-Read-Hall mechanism.[51] Under conditions of steady-state generation, and neglecting the diffusion of electrons, the optically generated excess electron concentration Δn satisfies the following equation:[52]

$$(\Delta n)^2 + (n_0 + p_0 - \tau_h g)\Delta n = (n_0 + p_0)\tau_l g \ , \tag{4}$$

where τ_l and τ_h are the electron lifetime in the low- and high-injection limits, respectively. The symbols n_0 and p_0 denote the equilibrium electron and hole concentrations in the dark, respectively. Under our experimental conditions, the semiconductor is extrinsic, and we have $p_0 \approx N_A$ and $n_0 = n_i^2 / N_A$. The intrinsic carrier concentration n_i is given by[53]

$$n_i = \Upsilon T^{3/2} \exp(-E_i / kT) \ , \tag{5}$$

with $\Upsilon = 3.10 \times 10^{16}$ cm^{-3} K$^{-3/2}$ and $E_i = 0.603$ eV. The generation rate of electron-hole pairs at a depth w below the surface is given by

$$g = \phi \Gamma \alpha \exp(-\alpha w) \ , \tag{6}$$

where Γ is the Schottky contact transmittance ($\Gamma \approx 0.6$), α the absorption coefficient of the sample ($\alpha = 980$ cm^{-1}),[54] and ϕ the incident light intensity ($\phi = \gamma I_{ph}$, with $\gamma = 196$ mW cm^{-2} mA^{-1}). If $\tau_l > \tau_h$, the solution of Eq. (4) can be approximated by[52]

$$\Delta n = \tau_l g, \quad g \ll \frac{n_0 + p_0}{\tau_l} \ ; \tag{7a}$$

$$\Delta n = \sqrt{g \tau_l (n_0 + n_0)}, \quad \frac{n_0 + p_0}{\tau_l} \ll g \ll \frac{n_0 + p_0}{\tau_h^2} \tau_l \ ; \tag{7b}$$

$$\Delta n = \tau_h g, \quad g \gg \frac{n_0 + p_0}{\tau_h^2} \tau_l \ . \tag{7c}$$

The dependence of r on I_{ph} in the weakly doped samples (Fig. 8) is consistent with Eqs. (7a) and (7b) if we assume that

$$r = cn = c(n_0 + \Delta n) \ , \tag{8}$$

where c only depends on the temperature. Indeed, if $n_0 \ll \Delta n$ ($n_0 = 6.6 \times 10^{12}$ cm^{-3} at 160 °C) Δn and $r \approx cn$ vary linearly with g or (I_{ph}) in the low-injection regime [Eq. (7a)] and are proportional to $\sqrt{g}$ [or $(I_{ph})^{1/2}$] in the high-injection regime [Eq. (7b)]. The transition from the low- to the high-injection condition occurs at $I_{ph} = I_{ph}^t \approx 0.1$ mA (Fig. 8) which corresponds to $g = g^t = 3 \times 10^{19}$ cm^{-3} s^{-1}, and determines the lifetime

$$\tau_l = (n_0 + p_0)/g^t \approx 4 \ \mu\text{s} \ .$$

We calculate the exact value of Δn versus I_{ph} by solving Eq. (4) with $\tau_l = 4$ μs, and $\tau_h = 0.4$ μs (Fig. 8, upper horizontal scale). At each temperature, we fit the experimental values of r to Eq. (8) by adjusting the parameter c. The calculated curves (solid and dashed lines in Fig. 8) agree well with the experimental data in the I_{ph} interval for which the fit is performed (solid part of the lines). The values of c follow the Arrhenius equation $c = c_0 \exp(-E_c^f / kT_a)$, with $E_c^f = 1.1 \pm 0.1$ eV, and $c_0 = 4 \times 10^{10}$ s^{-1} (Fig. 12). The calculated dependence of r on I_{ph} shows no influence on τ_h provided the condition

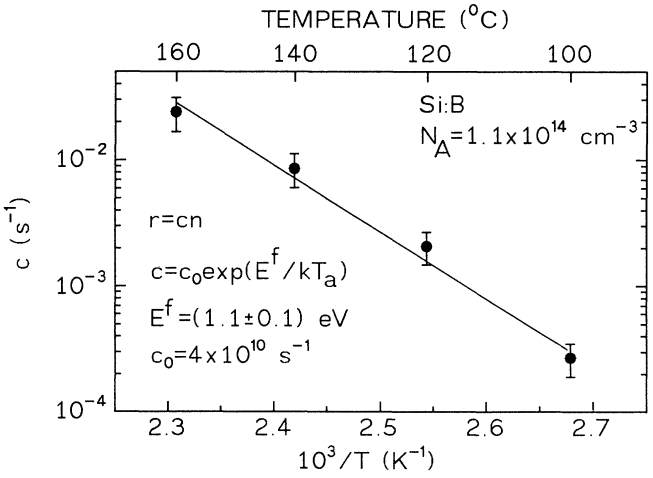

FIG. 12. Arrhenius plot of the values of c obtained by fitting the data of Fig. 8 to the equation $r = cn$. The solid line represents a fit of the values of c to the specified Arrhenius equation.

$\tau_h < \tau_l/10$ is fulfilled; otherwise, a linear dependence of Δn on I_{ph} occurs for $I_{ph} < 10$ mA [Eq. (7c)], in contradiction with the experimental data. The fits agree with the experimental data at all temperatures provided τ_l is in the range from $\tau_{l\,min} = 1$ μs to $\tau_{l\,max} = 10$ μs.

In the more highly doped samples ($N_A = 4.0 \times 10^{15}$ cm^{-3} and $N_A = 3.8 \times 10^{16}$ cm^{-3}), the low-injection condition

$$g \ll (n_0 + p_0)/\tau_l \approx N_A/\tau_l$$

is fulfilled even at the highest photocurrent (10 mA), and we expect a linear dependence of r on I_{ph}, which is indeed observed (Fig. 7).

The small spread of r for different values of N_A (Fig. 7) give strong evidence that τ_l is the same in all samples. The lifetime $\tau_l = 4$ μs corresponds to a diffusion length of ≈ 70 μm, which is much larger than the light absorption depth $1/\alpha \approx 10$ μm. Therefore, τ_l should be considered as an effective lifetime, which is strongly influenced by surface recombination processes. The smaller value of r in the samples without HNO_3 treatment might be explained by a smaller lifetime τ_l due to a larger density of surface states. The thin oxide layer generated by the HNO_3 treatment probably decreases the surface recombination velocity by passivating surface states.

Under the short-circuit conditions the photogenerated electrons diffuse toward the contact which acts as a perfect sink. The electron concentration, and, consequently, the annealing rate r, are smaller than in the open-circuit configuration.

We directly determine the lifetime τ_l using the open-circuit voltage-decay method.[55] We record the open-circuit voltage V_{oc} as a function of time after the turnoff of the laser diode. In the exponential decay regime—which occurs at low values of V_{oc}—the time constant τ_d is equal to the minority carrier lifetime. We find $\tau_d = (10 \pm 7)$ μs, in reasonable agreement with $\tau_l = 4$ μs derived from the data in Fig. 8. The decay time τ_d does not depend on the temperature ($T = 100$–180 °C) nor on N_A within the experimental accuracy.

The dashed part of the lines in Fig. 8 clearly shows that Eq. (8) does not hold for $I_{ph} < 10^{-2}$ mA. We conclude therefore that the annealing mechanism in the dark and under illumination is different.

In summary, items (2) and (3) of Sec. III D can be replaced by the following statements.

(a) The annealing parameter under strong illumination ($I_{ph} > 0.1$ mA) r^l is proportional to the electron concentration n, and is thermally activated with an activation energy $E_r^l = 1.1 \pm 0.1$ eV.

(b) In the dark, the relation $r = cn_0$ does not hold, and the thermal activation energy of r is $E_r^d = 1.75 \pm 0.06$ eV.

B. Kinetic model

The dissociation and formation of BH pairs are described by the following reaction and kinetic equation:

$$BH \rightleftharpoons B^- + H^+ , \tag{9}$$

$$\frac{d[BH]}{dt} = \sigma_B a [H](N_A - [BH]) - \nu_B [BH] , \tag{10}$$

where [H] and [BH] are the concentrations of free atomic hydrogen and BH complexes, respectively; σ_B is the capture parameter of a positively charged hydrogen atom by a free acceptor; a is the fraction of the positively charged hydrogen ($a = [H^+]/[H]$); and ν_B is the dissociation frequency of the BH complex. The capture of neutral H at the B atom is negligible due to the lack of Coulombic attraction. If only reaction (9) occurs, [H]+[HB] is constant and does not depend on the temprature T. We measure the net inactive boron concentration $R = N_A - N_I = a[H] + [HB]$ at room temperature in the dark. We will show in Sec. IV C that $a \approx 1$ and $[H] \ll [BH]$ under the measurement conditions. Therefore,

$$R \approx [HB](T = 300\ K) = [H] + [HB]$$

at any temperature.

The reactivation of the boron acceptor requires that H is either removed by long-range migration or converted into an electrically inactive state. As already pointed out in Sec. III, the profiles of Figs. 1, 3, and 5 do not support an annealing mechanism which is limited by H outdiffusion.

The fact that Eq. (3) reduces to a second-order equation [Eq. (2)] for long annealing times suggests that the annealing kinetics are rate limited by the following bimolecular reaction:

$$H + H \rightarrow \tilde{H}_2 . \tag{11}$$

The symbol $\tilde{H}_2$ denotes an electrically inactive complex which involves two H atoms, but is not necessarily identical with the hydrogen molecule H_2. The complex $\tilde{H}_2$ has to be stable up to at least the highest annealing temperature in our experiments (220 °C). In a first step it is not necessary to take into account the charge state of H. The corresponding kinetic equation will then be

$$\frac{d[\tilde{H}_2]}{dt} = \sigma_H [H][H] , \tag{12}$$

where σ_H is the second-order $\tilde{H}_2$ formation rate. If the long-range hydrogen diffusion is negligible, the total H concentration

$$H_T = [BH] + [H] + 2[\tilde{H}_2]$$

does not change with the annealing time, and

$$2\frac{d\tilde{H}_2}{dt} = -\frac{d([BH]+[H])}{dt} = -\frac{dR}{dt} . \tag{13}$$

Thus Eq. (12) can be rewritten

$$\frac{dR}{dt} = -2\sigma_H [H][H] . \tag{14}$$

To derive a relation between $R = [BH] + [H]$ and [H], we assume that reaction (9) is much faster than (11). Dynamic equilibrium is then achieved for (9), i.e., $d[BH]/dt = 0$, and (10) becomes

$$a[\mathrm{H}]^2+[a(N_A-R)+K][\mathrm{H}]-KR=0 \ . \tag{15}$$

The equilibrium constant of reaction (9), $K=\nu_B/\sigma_B$, satisfies the Arrhenius expression $K=K_0\exp(-E_B/kT)$, where E_B represents the binding energy of the BH complex. We derive [H] from Eq. (15) by neglecting the term $a[\mathrm{H}]^2$, and assuming that $a(N_A-R)\gg K$:

$$[\mathrm{H}]=\frac{K}{a}\frac{R}{(N_A-R)} \ . \tag{16}$$

The condition $a(N_A-R)\gg K$ implies that most of the hydrogen is trapped at the boron atoms ($[\mathrm{H}]\ll[\mathrm{BH}]$). Substituting (16) in (14), we obtain

$$\frac{dR}{dt}=-2\sigma_H\left[\frac{K}{a}\right]^2\frac{R^2}{(N_A-R)^2} \ , \tag{17}$$

which is equivalent to Eq. (3) with

$$r=2\left[\frac{K}{a}\right]^2\sigma_H \ . \tag{18}$$

We now derive expressions for r under illumination and in the dark which are consistent with statements (a) and (b) of Sec. IV A. We assume that H in p-type silicon has a neutral state H^0, and a positively charged state H^+. The ratios $a=[H^+]/[H]$ and $b=[H^0]/[H]$ are determined by the hydrogen donor level located above midgap at an energy ΔE below the conduction band:

$$a=\frac{[H^+]}{[H]}=1-b \ , \tag{19}$$

$$b=\frac{[H^0]}{[H]}=\left[1+\frac{N_c}{\xi n}\exp\left[-\frac{\Delta E}{kT}\right]\right]^{-1} \ . \tag{20}$$

The symbols N_c and ξ denote the effective density of states in the conduction band and the ground-state degeneracy of the donor level ($\xi=2$), respectively.

Taking into account the different charge states of H, Eq. (11) can be written in three different ways:

$$H^+ + H^+ \rightarrow \tilde{H}_2 + 2h^+ \ , \tag{21a}$$

$$H^+ + H^0 \rightarrow \tilde{H}_2 + h^+ \ , \tag{21b}$$

$$H^0 + H^0 \rightarrow \tilde{H}_2 \ . \tag{21c}$$

The corresponding kinetic equations are

$$\frac{d[\tilde{H}_2]}{dt}=\sigma_H^{++}[H^+][H^+]=\sigma_H^{++}a^2[\mathrm{H}]^2 \ , \tag{22a}$$

$$\frac{d[\tilde{H}_2]}{dt}=\sigma_H^{+0}[H^+][H^0]=\sigma_H^{+0}ab[\mathrm{H}]^2 \ , \tag{22b}$$

$$\frac{d[\tilde{H}_2]}{dt}=\sigma_H^{00}[H^0]^2=\sigma_H^{00}b^2[\mathrm{H}]^2 \ , \tag{22c}$$

which are formally equivalent to Eq. (12). Using Eq. (18), we derive the kinetic parameters r associated to reactions (21a), (21b), and (21c):

$$r^{++}=2K^2\sigma_H^{++} \ , \tag{23a}$$

$$r^{+0}=2K^2\frac{b}{a}\sigma_H^{+0} \ , \tag{23b}$$

$$r^{00}=2K^2\frac{b^2}{a^2}\sigma_H^{00} \ . \tag{23c}$$

The second-order $\tilde{H}_2$ formation rates $\sigma_H^{i,j}$ ($i,j=+$ or 0) depend only on the temperature, and follow the Arrhenius equation

$$\sigma_H^{i,j}=\sigma_{0H}^{i,j}\exp(-E_H^{i,j}/kT) \ .$$

Equation (23b) predicts a linear dependence of r on the electron concentration n, provided the condition

$$[N_c/(\xi n)]\exp(-\Delta E/kT)\gg 1 \ ,$$

e.g., $b\ll 1$ is fulfilled. Then we have

$$b\approx n(\xi/N_c)\exp(\Delta E/kT)$$

and $a\approx 1$ from Eqs. (20) and (19), respectively, and

$$r^{+0}=n\frac{2\xi K^2\sigma_H^{+0}}{N_c}\exp\left[\frac{\Delta E}{kT}\right] \ . \tag{24}$$

In contrast, r^{++} does not depend on n, and r^{00} is proportional to n^2.

Equation (21b) describes the annealing mechanism under strong illumination ($I_{ph}>I_{ph}^{th}$), and $r^l=r^{+0}$. As the light intensity decreases below a threshold value ($I_{ph}<I_{ph}^{th}$), r^{+0} becomes smaller than r^{++}, reaction (21a) predominates over (21b), and the kinetic parameter in the dark is given by $r^d=r^{++}$.

Substituting the Arrhenius relation of K, and $\sigma^{i,j}$ in Eqs. (23a) and (24), we obtain the following expressions of the annealing parameter in the dark and under illumination:

$$r^d=2K_0^2\sigma_{0H}^{++}\exp\left[-\frac{E_H^{++}+2E_B}{kT}\right] \ , \tag{25}$$

$$r^l=n\frac{2\xi K_0^2\sigma_{0H}^{+0}}{N_c}\exp\left[-\frac{E_H^{+0}+2E_B-\Delta E}{kT}\right] \ . \tag{26}$$

We now compare the prefactors and the activation energies in the Arrhenius equations (25) and (26) with the experimental values.

C. Quantitative comparison of the model and the experimental data

Relations (25) and (26) are valid under the following assumptions: (i) Reaction (9) is in dynamical equilibrium, (ii) $a(N_A-R)\gg K$, i.e., $[\mathrm{H}]\ll[\mathrm{BH}]$, and (iii) $(N_c/\xi)n\exp(-\Delta E/kT)\gg 1$, i.e., $a\approx 1$ and $b\ll 1$.

We need an estimate of the parameters ΔE, E_H^{++}, E_H^{+0}, and E_B, which have not been accurately determined in the literature. The condition (iii) defines an upper limit of ΔE: $(\Delta E)_{min}=-kT_{max}\ln(\xi n_{max}/N_c)$. Taking $T_{max}=160\,^\circ\mathrm{C}$, $N_c=4\times10^{19}$ cm^{-3}, $\xi=2$, and $n_{max}=1\times10^{15}$ cm^{-3} (see Fig. 8), we find $\Delta E\approx 0.32$ eV. In the following we take the value $\Delta E=0.3$ eV.

Due to the lack of Coulombic interaction between H^0 and H^+, reaction (21b) is limited by the short-range mi-

gration of interstitial H, and the capture parameter is given by

$$\sigma_H^{+0}=8\pi R_H^{+0}D_H \ , \tag{27}$$

where R^{+0} is the capture radius ($R^{+0}\approx 2$ Å), D_H the diffusivity of atomic hydrogen. Theoretical investigations[32,33] predict very similar diffusion paths, and migration energies for H^0 and H^+, and we do not distinguish between the two charge states with regard to the diffusivity. No reliable measurements of D_H are available in the low-temperature range ($T<200$ °C). We use the values $D_{0H}=9.4\times10^{-3}$ cm^2/s, and $E_m=0.48$ eV derived from high-temperature permeation measurements.[56] In reaction (21a) the Coulombic repulsion between the two positively charged H atoms generates an additional energy barrier E_{cap} in the capture process which can be described by

$$\sigma_H^{++}=8\pi R_H^{++}D_H\exp\left[\frac{-E_{cap}}{kT}\right] . \tag{28}$$

We use the value of the BH complex binding energy $E_B=0.6\pm0.1$ eV determined by Herrero *et al.*[57] from the analysis of H diffusion profiles.

From Eqs. (25)–(28) we derive the following expressions for the activation energies E_r^d and E_r^l of the kinetic parameter r in the dark and under illumination:

$$E_r^d=E_m+E_{cap}+2E_B \ , \tag{29}$$

$$E_r^l=E_m+2E_B-\Delta E \ . \tag{30}$$

Equation (30) gives an activation energy E_r^l of 1.4 eV which agrees reasonably with the experimental value $\bar{E}_r^l=1.1\pm0.1$ eV in view of the large error on E_m, E_B, and ΔE. Substituting the experimental value $\bar{E}_r^d=1.75\pm0.06$ eV in Eq. (29), we find a capture barrier $E_{cap}=0.1\pm0.4$ eV.

According to Eqs. (25)–(28), the prefactors in the Arrhenius equations of r^d and c ($r=cn$ under strong illumination) are given by

$$r_0^d=16\pi K_0^2 D_{0H}R_H^{++} \ , \tag{31}$$

$$c_0=\frac{16\pi K_0^2\xi D_{0H}R_H^{+0}}{N_c} \ . \tag{32}$$

Under the assumption $R_H^{++}\approx R_H^{+0}$, the ratio $r_0^d/c_0=\xi/N_c$ is 2×10^{19} cm^3, which agrees reasonably with the experimental value of 5×10^{21} cm^{-3} determined in the 120-Ω cm samples ($r_0^d=2\times10^{32}$ cm^{-3}/s from Table I and $c_0=4\times10^{10}$ s^{-1} from Fig. 12). The error on the prefactors is at least an order of magnitude. We substitute the experimental value $r_0^d=2\times10^{32}$ cm^{-3}/s in Eq. (31) and we find $K_0=1\times10^{20}$ cm^{-3}. At the same time, however, K_0 equals ν_{0B}/σ_{0B}, where ν_{B0} and σ_{B0} are the prefactors of the Arrhenius expression ν_B and σ_B, respectively. We find $K_0\approx6\times10^{21}$ cm^{-3} taking[23] $\sigma_B=4\pi R_B D_{H0}$, $R_B=40$ Å, and $\nu_{B0}=3\times10^{14}$ s^{-1}. The discrepancy between the two values lies within the experimental error.

The upper limit of K_0 defined by condition (ii) is

$$(K_0)_{max}=a(N_A-R)_{min}\exp(E_B/kT_{max}) \ . \tag{33}$$

Using $a\approx1$, $(N_A-R)_{min}\approx4\times10^{13}$ cm^{-3} (see Fig. 3), and $T_{max}=180$ °C, we find $(K_0)_{max}=2\times10^{20}$ cm^{-3} which is consistent with the value $K_0=3\times10^{20}$ cm^{-3} derived from Eq. (31).

We solve analytically Eq. (10) and calculate [BH] as a function of time taking $\nu_B=K\sigma_B$, $K_0=3\times10^{20}$ cm^{-3}, and $E_B=0.6$ eV. At each temperature the complex concentration reaches an equilibrium value within a time which is negligible compared to the annealing time in our investigations. Therefore, dynamical equilibrium is always achieved for reaction (9).

We have presented a set of parameters $\Delta E=0.3$ eV, $E_B=0.6$ eV, $E_m=0.48$ eV, $K_0=3\times10^{20}$ cm^{-3}, and $D_{0H}=9.4\times10^{-3}$ cm^2/s which allows us to determine the activations energies E_r^d, E_r^l, and prefactors r_0^d, r_0^l in full agreement with the experimental data. The conditions (i)–(iii) are fulfilled, and the model is consistent.

V. DISCUSSION

We compare our data with results obtained from annealing experiments on samples which are hydrogenated via avalanche electron injection[25] (AEI), electron-beam irradiation[24] (EBI), or low-energy ion implantation.[26] In these experiments the change in the electrically inactive boron concentration as a function of the annealing time shows an initial first-order step followed by a long-time second-order process. The identification of the fast initial step as a first-order process[24,25] is uncertain due to its short duration.[26] Our modified kinetic reaction defined by Eq. (3) properly describes the whole annealing process. Furthermore, the parameters r' and r derived from the analysis of the data according to Eqs. (2) and (3) satisfy the relation $r=r'N_A^2$ for N_A varying over more than two orders of magnitude. (See Sec. III.) These facts provide strong evidence that the second-order kinetics are only an approximation of the accurate process defined by Eq. (3). In the model proposed by Sah *et al.*,[25] two different reactions successively occur during the annealing process. In contrast, we show that the formation of diatomic complexes is the rate-limiting reaction even at short times. The fast initial step is not controlled by the formation and dissociation of BH complexes,[25] but results from conditions (i) and (ii) in Sec. IV C, i.e., reaction (9) equilibrates rapidly, and the BH complex dissociation is incomplete ([H]$\ll$[BH]).

The second-order parameter r' in the dark has been previously determined in samples which are hydrogenated via low-energy implantation,[26] avalanche electron injection,[25] or electron-beam irradiation.[24] We compare the product $r=r'N_A^2$ from these references to the value of r measured in this work. The values of $r'N_A^2$ from the H-implanted samples[26] with $N_A=1.5\times10^{15}$ cm^{-3} (Fig. 10, rhombus) reasonably agree with the data in our plasma-treated samples. The annealing parameters $r'N_A^2$ measured in the AEI (Ref. 25) and EBI (Ref. 24) samples are more than three orders of magnitude larger than r in our plasma-treated samples. The reason for this discrepancy is not clear, but the data from the AEI and

EBI samples are the less reliable ones, due to the poor linearity of the plots $1/R$ versus t_a (see Ref. 25, Fig. 3b, and Ref. 24, Fig. 2b).

The occurrence of the factor $(N_A - R)^{-2}$ in the kinetic equation (3) implies that $\eta = [\mathrm{H}]/[\mathrm{BH}]$ is much smaller than unity under the annealing conditions of this work. [See Eqs. (14)–(16).] The ratio η decreases with temperature, and the free H concentration might be below the detection limit of the most sensitive methods of characterization. Hence the H donor level is not observed either as a majority or as a minority carrier trap in a DLTS (deep-level transient spectroscopy) experiment.

The linear dependence of the annealing parameter r^l on the electron concentration is fully consistent with Eq. (21b). The neutral H^0 atom results from the reaction $\mathrm{H}^+ + \rightleftharpoons \mathrm{H}^0$, which is controlled by the H donor level located at an energy $\Delta E < 0.35$ eV below the conduction band. We rule out the reaction $\mathrm{H}^+ + \mathrm{H}^- \rightleftharpoons \tilde{\mathrm{H}}_2$, which involves the capture of two electrons and gives a quadratic dependence of r^l on the electron concentration. The annealing processed under illumination requires neutral hydrogen, and is not consistent with the negative U property predicted by the calculations of Van de Walle *et al.*[33] These calculations,[33] however, cannot totally exclude the occurence of H^0. The model requires that $b = [\mathrm{H}^0]/[\mathrm{H}]$ is much less than unity for any annealing condition. The ratio b increases with the light intensity and decreases with temperature. We conclude that hydrogen is predominantly in the positive charge state in p-type Si. In particular, this holds in the space-charge region of a reverse-biased diode, in agreement with the drift property of hydrogen.[23,26,27,45–47]

The kinetics defined by Eq. (3) require that the annealing process is limited by the formation of an electrically *inactive* complex $\tilde{\mathrm{H}}_2$ which involves *two* H atoms and is *stable* at least up to 200 °C. The properties required for the $\tilde{\mathrm{H}}_2$ species are identical to those of the highly immobile, stable, and neutral H-related entity observed by Johnson and Herring[27] in reverse-bias n^+p junction treated in an H plasma. The authors suggest that this entity is a H_2 molecule which forms according to the reaction $\mathrm{H}^+ + \mathrm{H}^0 \rightarrow \mathrm{H}_2 + h^+$, but there is no direct evidence that only two H atoms are involved in the defect.[27] A possible candidate for the $\tilde{\mathrm{H}}_2$ defect could be the $(\mathrm{H}_{BC}\mathrm{H}_{AB})$ complex which is predicted by theory.[37,38] This stable and immobile defect consists of two H atoms located at adjacent bond-center and antibonding lattice sides. It is formed according to the reaction[37] $(\mathrm{H}^+)_{BC} + (\mathrm{H}^0)_{AB} \rightarrow (\mathrm{H}_{BC}\mathrm{H}_{AB}) + h^+$, in agreement with our Eq. (21b).

VI. SUMMARY

We have investigated the reactivation of the boron acceptor in Schottky diode structures annealed in the dark or under illumination ($h\nu = 1.54$ eV) in the open-circuit configuration. The reactivation kinetics satisfy Eq. (3) over the entire range of the annealing process in the dark as well as under illumination. The annealing rate $dR/dt \approx d[\mathrm{BH}]/dt$ strongly decreases as the total acceptor concentration N_A increases, and the term $R^2/(N_A - R)^2$ in Eq. (3) entirely accounts for this dependence, e.g., the annealing parameter r does not depend on N_A. The B reactivation is strongly enhanced by illumination, provided the light intensity ϕ exceeds a threshold value ($I_{\mathrm{ph}}^{\mathrm{th}} \sim 10^{-2}$ mA). The kinetic parameter under illumination r^l increases linearly with ϕ in the low-injection regime, and is proportional to $\sqrt{\phi}$ in the high-injection regime. This dependence on ϕ proves that r^l is proportional to the electron concentration n. The kinetic parameters in the dark and under strong illumination are thermally activated with an activation energy of $\bar{E}_r^d = 1.75 \pm 0.06$ eV and $\bar{E}_r^l = 1.1 \pm 0.1$ eV, respectively.

The kinetics defined by Eq. (3) result from two chemical reactions: (a) the dissociation and formation of the BH complex which is in dynamical equilibrium and is much faster than (b) the formation of a diatomic hydrogen complex $\tilde{\mathrm{H}}_2$. In the dark, the reaction $\mathrm{H}^+ + \mathrm{H}^+ \rightarrow \tilde{\mathrm{H}}_2 + 2h^+$ controls the $\tilde{\mathrm{H}}_2$ formation, and the annealing rate is small due to the Coulombic repulsion between the protons. The electron concentration strongly increases under illumination, and a small fraction of H^+ converts into H^0. The kinetics are limited by reaction $\mathrm{H}^+ + \mathrm{H}^0 \rightarrow \tilde{\mathrm{H}}_2 + h^+$ which is consistent with the linear dependence of r^l on n. Our analysis provides evidence for an H donor level located above midgap and the existence of a neutral charge state for H. The ratio $[\mathrm{H}]/[\mathrm{BH}]$ is much less than unity, and most of the remaining free H is in the positive charge state.

ACKNOWLEDGMENTS

We acknowledge stimulating discussions with H. J. Queisser, M. Stutzmann, J. Werner, M. Schulz, and T. Prescha. We appreciate the help of L. Tilly and G. Hofmann in performing some experiments, and the technical assistance of W. Heinz and W. Krause. We would like to thank L. Pasemann and C. Harris for useful remarks on the manuscript.

[1] S. J. Pearton, J. W. Corbett, and T. S. Shi, Appl. Phys. A **43**, 153 (1987).

[2] *Hydrogen in Semiconductors,* edited by J. I. Pankove and M. N. Johnson, Vol. 34 of *Semiconductors and Semimetals* (Academic, New York, in press).

[3] J. I. Pankove, P. J. Zanzucchi, C. W. Magee, and G. Lucovsky, Appl. Phys. Lett. **46**, 421 (1985).

[4] N. M. Johnson, Phys. Rev. B **31**, 5525 (1985).

[5] Du Yong-Chang, Zhang Yu-Feng, Qin Guo-Gang, and Wong Shi-Fu, Solid State Commun. **55**, 501 (1985).

[6] B. Pajot, A. Chari, M. Aucouturier, M. Astier, and A. Chantre, Solid State Commun. **67**, 855 (1988).

[7] M. Stavola, S. J. Pearton, J. Lopata, and W. C. Dautremont-Smith, Phys. Rev. B **37**, 8313 (1988).

[8] M. Stavola, S. J. Pearton, J. Lopata, and W. C. Dautremont-Smith, Appl. Phys. Lett. **50**, 1086 (1987).

[9] M. Stavola, K. Bergman, S. J. Pearton, and J. Lopata, Phys. Rev. Lett. **24**, 2786 (1988).

[10] M. Stutzmann, Phys. Rev. B **35**, 5921 (1987).

[11] M. Stutzmann and C. P. Herrero, Phys. Scr. **T25**, 276 (1989).

[12]C. P. Herrero and M. Stutzmann, Solid State Commun. **68**, 1085 (1988).
[13]M. L. W. Thewalt, E. C. Lightowlers, and J. I. Pankove, Appl. Phys. Lett. **46**, 689 (1985).
[14]A. D. Marwick, G. S. Oehrlein, and N. M. Johnson, Phys. Rev. B **36**, 4539 (1987).
[15]B. B. Nielsen, J. U. Andersen, and S. J. Pearton, Phys. Rev. Lett. **60**, 321 (1988).
[16]Th. Wichert, H. Skudlik, M. Deicher, G. Grübel, R. Keller, E. Recknagel, and L. Song, Phys. Rev. Lett. **59**, 2087 (1987).
[17]G. G. DeLeo and W. B. Fowler, Phys. Rev. B **31**, 6861 (1985).
[18]K. J. Chang and D. J. Chadi, Phys. Rev. Lett. **60**, 1422 (1988).
[19]P. J. H. Denteneer, C. G. Van de Walle, and S. T. Pantelides, Phys. Rev. B **39**, 10 809 (1989).
[20]T. Sasaki and H. Katayama Yoshida, in *Proceedings of the Fifteenth International Conference on Defects in Semiconductors, Hungary, 1988,* Materials Science Forum, Vols. 38–41, edited by G. Ferenczi (Trans Tech, Ch. Aedermannsdorf, Hungary, 1989), p. 973.
[21]S. K. Estreicher, L. Throckmorton, and D. S. Marynick, Phys. Rev. B **39**, 13 241 (1989).
[22]A. A. Bonapasta, A. Lapiccirella, N. Tomassini, and M. Capizzi, Phys. Rev. B **36**, 6228 (1987).
[23]T. Zundel and J. Weber, Phys. Rev. B **39**, 13 549 (1989).
[24]S. C. S. Pan and C. T. Sah, J. Appl. Phys. **60**, 156 (1986).
[25]C. T. Sah, S. C. S. Pan, and C. C. H. Hsu, J. Appl. Phys. **57**, 5148 (1985).
[26]T. Zundel, A. Mesli, J. C. Muller, and P. Siffert, Appl. Phys. A **48**, 31 (1989).
[27]N. M. Johnson and C. Herring, Phys. Rev. B **38**, 1581 (1988).
[28]D. Mathiot, Phys. Rev. B **40**, 5867 (1989).
[29]R. N. Hall, in *Proceedings of the Thirteenth International Conference on Defects in Semiconductors,* edited by L. C. Kimerling and J. M. Parsey Jr. (Metallurgical Society, American Institute of Mechnical Engineers, Wavendale, PA, 1985), Vol. 14a, p. 759.
[30]M. Capizzi, A. Mittiga, and A. Frova, in *Proceedings of the Eighteenth International Conference on Defects in Semiconductors,* edited by O. Engström (World Scientific, Singapore, 1987), Vol. 2, p. 995.
[31]J. T. Borenstein, D. Tulchinski, and J. W. Corbett, in *Impurities, Defects and Diffusion in Semiconductors: Bulk and Layered Structures,* Proceedings of the Materials Research Society, edited by D. J. Wolford, J. Bernholc, and E. E. Haller (Materials Research Society, Pittsburgh, PA, 1990), Vol. 163, p. 633.
[32]P. Deak, L. C. Snyder, and J. W. Corbett, Phys. Rev. B **37**, 6887 (1988).
[33]C. G. Van de Walle, P. J. H. Denteneer, Y. Bar-Yam, and S. T. Pantelides, Phys. Rev. B **39**, 10 791 (1989).
[34]A. Mainwood and A. M. Stoneham, J. Phys. C **17**, 2513 (1984).
[35]T. S. Shi, S. N. Sahu, J. W. Corbett, and L. C. Snyder, Sci. Sin. **27**, 98 (1984).
[36]J. M. Baranowski, Phys. Rev. B **39**, 8616 (1989).
[37]P. Deak and L. C. Snyder, Radiation Effects and Defects in Solids **111-112**, 77 (1989).
[38]K. J. Chang and D. J. Chadi, Phys. Rev. Lett. **62**, 937 (1989).
[39]B. B. Nielsen, Phys. Rev. B **37**, 6353 (1988).
[40]Yu. V. Gorelkinskii and N. N. Nevinnyi, Pis'ma Zh. Tekh. Fiz. **13**, 105 (1987) [Sov. Tech. Phys. Lett. **13**, 45 (1987)].
[41]R. F. Kiefl, M. Celio, T. L. Estle, S. R. Kreitzman, G. M. Luke, T. M. Riseman, and E. J. Ansaldo, Phys. Rev. Lett. **60**, 224 (1988).
[42]S. Estreicher, Phys. Rev. B **36**, 9122 (1987).
[43]G. G. DeLeo, M. J. Dorogi, and W. Beall Fowler, Phys. Rev. B **38**, 7520 (1988).
[44]A. Amore Bonapasta, A. Lapiccirella, N. Tomassini, and M. Capizzi, Europhys. Lett. **7**, 145 (1988).
[45]A. J. Tavendale, D. Alexiev, and A. A. Williams, Appl. Phys. Lett. **47**, 316 (1985).
[46]A. J. Tavendale, A. A. Williams, and S. J. Pearton, Appl. Phys. Lett. **48**, 590 (1986).
[47]A. J. Tavendale, A. A. Williams, D. Alexiev, and S. J. Pearton, in *Oxygen, Carbon, Hydrogen and Nitrogen in Crystalline Silicon,* Proceedings of the Materials Research Society, edited by J. C. Mikkelsen, Jr., S. J. Pearton, J. W. Corbett, and S. J. Pennycook (Materials Research Society, Pittsburgh, PA, 1986), Vol. 59, p. 469.
[48]M. Capizzi and A. Mittiga, Appl. Phys. Lett. **50**, 918 (1987).
[49]S. T. Pantelides, Appl. Phys. Lett. **50**, 995 (1987).
[50]N. M. Johnson and C. Herring, in *Proceedings of the Fifteenth International Conference on Defects in Semiconductors, Hungary, 1988,* Materials Science Forum, Vols. 38–41, edited by G. Ferenczi (Trans Tech, Ch. Aedermannsdorf, Hungary, 1989), p. 961.
[51]R. N. Hall, Solid State Electron. **24**, 595 (1981).
[52]J. S. Blakemore, *Semiconductor Statistics* (Dover, New York, 1987), pp. 262–273.
[53]C. D. Thurmond, J. Electrochem. Soc. **112**, 1133 (1975).
[54]W. C. Dash and R. Newman, Phys. Rev. **99**, 1151 (1955).
[55]J. E. Mahan, T. W. Ekstedt, R. I. Frank, and R. Kaplow, IEEE Trans. Electron Devices **ED-26**, 733 (1979).
[56]A. Van Wieringen and N. Warmoltz, Physica **22**, 849 (1956).
[57]C. P. Herrero, M. Stutzmann, A. Breitschwerdt, and P. V. Santos, Phys. Rev. B **41**, 1054 (1990).